All-optical switching of silicon disk resonator based on photothermal effect in metal–insulator–metal absorber

Yuechun Shi,[1,2,†] Xi Chen,[1,†] Fei Lou,[1] Yiting Chen,[1] Min Yan,[1] Lech Wosinski,[1] and Min Qiu[1,3,*]

[1]*Optics and Photonics, School of Information and Communication Technology, KTH—Royal Institute of Technology, Electrum 229,16440 Kista, Sweden*

[2]*Nanjing National Laboratory of Microstructures, Microwave-Photonics Technology Laboratory, Nanjing University, 210093 Nanjing, China*

[3]*State Key Laboratory of Modern Optical Instrumentation, Department of Optical Engineering, Zhejiang University, 310027 Hangzhou, China*

**Corresponding author: minqiu@zju.edu.cn*

Received May 6, 2014; revised June 7, 2014; accepted June 16, 2014; posted June 20, 2014 (Doc. ID 211493); published July 23, 2014

Efficient narrowband light absorption by a metal–insulator–metal (MIM) structure can lead to high-speed light-to-heat conversion at a micro- or nanoscale. Such a MIM structure can serve as a heater for achieving all-optical light control based on the thermo-optical (TO) effect. Here we experimentally fabricated and characterized a novel all-optical switch based on a silicon microdisk integrated with a MIM light absorber. Direct integration of the absorber on top of the microdisk reduces the thermal capacity of the whole device, leading to high-speed TO switching of the microdisk resonance. The measurement result exhibits a rise time of 2.0 μs and a fall time of 2.6 μs with switching power as low as 0.5 mW; the product of switching power and response time is only about 1.3 mW · μs. Since no auxiliary elements are required for the heater, the switch is structurally compact, and its fabrication is rather easy. The device potentially can be deployed for new kinds of all-optical applications.

OCIS codes: (130.4815) Optical switching devices; (250.5403) Plasmonics; (130.3120) Integrated optics devices; (190.4870) Photothermal effects.

http://dx.doi.org/10.1364/OL.39.004431

Silicon photonics is one of the most promising technologies for future photonic integrated circuits because of low loss light propagation, high integration density, and compatibility with complementary metal-oxide-semiconductor (CMOS) fabrication platforms [1,2]. We have recently witnessed several breakthroughs in silicon photonics, such as silicon modulators [3–5], hybrid semiconductor lasers [6–8], and detectors [9–11]. However, dynamically controlling light flow in a silicon chip with a small footprint, which is usually realized by means of shifting the resonant or transmission peak using elements such as a microring, microdisk, and Mach–Zehnder interferometer (MZI) to realize switching, modulation, or routing, still remains a challenge due to the small electro-optic effect of silicon material. Several methods have been proposed to overcome the problem, such as electrically driven modulation of a microring resonator using the charge carrier injecting effect [12], all-optical control of a silicon ring using an optical nonlinear effect [13], and electrically driven thermo-optical (TO) switching devices [14–19]. The TO effect, which is usually realized by heating an optical device with an electrically driven thin film heater, is widely chosen as an efficient method for on-chip control of optical signals because of the large thermo-optical coefficient of silicon (Si) and the CMOS compatible fabrication procedure. However, light controlling using electrical heaters suffers from the drawbacks of low response time as well as high power consumption, owing to the slow thermal conduction of such a device. Many efforts have been made to solve the problem, including the differential control method [14,15]. Recently, Watts *et al.* reported on their MZI switch, which utilizes an adiabatic bend to inject current directly into the Si waveguides for efficient heating [20]. A fast response time of 2.4 μs with a low power-time product of 30.5 mW · μs was achieved. It also clarifies that in order to improve the temporal response and reduce power consumption, the heat capacity of the whole element and the required temperature increase for phase shift have to be reduced. Further, the authors applied the proposed heater to successfully demonstrate a tunable photonic phase array [21]. But the improved performance of their switch comes at the cost of a complex structure and a demanding fabrication process.

On the other hand, recently proposed metal–insulator–metal (MIM) light absorbers [22–24] can almost perfectly convert an incident light in a narrow frequency band to heat. Therefore, the absorbers can serve as perfect optically controlled heaters for dynamical tuning of a silicon index. Compared with electrical heaters, optical heaters have compact sizes and ease of integration on silicon components. In fact, it is possible to fabricate a MIM absorber directly on top of silicon devices, without deteriorating optical mode(s) propagating in the silicon device. The small heat capacity of the device can lead to better temporal response. In this Letter, as an example, we experimentally demonstrate a TO all-optical switch based on a silicon microdisk with an integrated MIM light absorber. The absorber is deposited and patterned directly on top of the silicon microdisk to ensure efficient heat transfer. Despite its elementary structure, the switch has a response time close to the state-of-art performance of the electrically driven adiabatic silicon TO switch with a complex structure [20]. Since our design requires no

auxiliary elements, such as the contact electrode pad and isolated oxide cladding layer, the proposed structure is easy to fabricate. Such photothermal controlling of light may open a new way for various all-optical applications such as all-optical signal processing, remote optical switching of optical circuits, wireless sensors, chip-to-chip interconnects, etc.

The device was fabricated on a silicon-on-insulator (SOI) wafer with a 250 nm thick silicon top layer on a 3 μm thick buried silicon dioxide layer. As shown in Fig. 1(a), it consists of a silicon microdisk with a diameter of 16 μm and a silicon strip waveguide with 450 nm width and 250 nm thickness for single mode propagation. A 200 nm air gap between the microdisk and the strip waveguide was designed for coupling of the probe light. A MIM film with a 10 μm diameter was fabricated on the microdisk to efficiently absorb the pump light. As shown in Fig. 1(a), the absorber consists of 20 and 60 nm thick Au layers on the top and bottom, respectively. A 240 nm thick Al_2O_3 layer is sandwiched between these two Au layers.

In addition, a pair of nonuniform grating couplers was also fabricated at the two ends of the strip waveguide for coupling probe light from the input fiber to the waveguide with a 45 deg incidence angle and vice versa for outcoupling to the output fiber. The large tilt angles of the fiber tips leave enough space on top of the absorber for placing the objective lens, which focuses the pump beam on the sample.

The fabrication procedure is as follows. First, we fabricated the shallow-etched grating patterns on the SOI wafer by electron-beam lithography (EBL) and inductively coupled plasma (ICP) etching. Then another step of EBL and ICP etching was used to define the microdisk and waveguide structures. Subsequently, the MIM absorber was directly fabricated on top of the microdisk by EBL, e-beam physical vapor deposition, and a step of lift-off. Figure 1(b) shows the scanning electron microscope (SEM) picture of the fabricated MIM absorber integrated (MAI) Si disk.

Figure 2(a) shows the measured absorption spectra of the fabricated MIM absorbers. The MIM continuous film absorber shows a peak absorbance of 0.79 at the wavelength of 1020 nm with a full width at half-maximum (FWHM) of 69.7 nm. To compare, the MIM absorber with the 10 μm diameter disk pattern has a peak absorbance of 0.9 at the wavelength of 1040 nm, with a wider FWHM of 158.5 nm. The broadening of the absorption peak may be due to the imperfect layered structure at the edge of the MIM disks. The absorbance of MIM absorbers with a disk

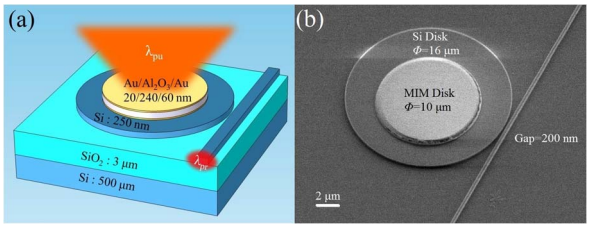

Fig. 1. (a) Diagram of SOI microdisk resonator integrated with a MIM absorber disk on top. (b) SEM image of the MIM absorber integrated Si disk coupled to a straight waveguide.

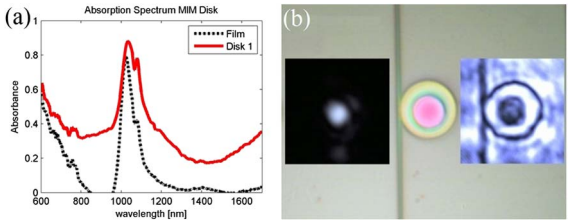

Fig. 2. (a) Measured absorption spectra of MIM absorbers. (b) Optical microscopic bright-feld image of MAI Si disk. The inset on the left side is the laser pump beam profile, with a Gaussian waist of 4.6 μm. The inset on the right side is the near-infrared dark field image of the MAI Si disk, where the MIM absorber is clearly shown as a darker round region in the center.

pattern is around 0.75 at 1064 nm, which is the wavelength of pump light in our later characterization. In Fig. 2(b), the visible light bright-field microscopic image shows that the MIM absorber has a pink color, which is due to the absorption of the MIM absorber in the visible spectrum.

The transmission spectra of the device were measured by using a tunable continuous wave fiber laser as a probe light and an optical spectrum analyzer as a detector. A Nd:YAG laser with a wavelength of 1064 nm was used as the pump light source. The sample stage was equipped with a thermoelectric controller (TEC) for stabilizing the surrounding temperature. The device was photothermally heated by a pump beam spot, with a Gaussian beam waist of 4.6 μm, as shown in the left inset of Fig. 2(b). In the right inset of Fig. 2(b), the near-infrared bright-field image shows that light at a wavelength of 1064 nm is effectively absorbed by the MIM absorber, as the MIM absorber appears much darker than the surrounding material of Si or SiO_2.

The measured transmission spectrum of the microdisk is shown in Fig. 3. As indicated in Fig. 3(a), the free spectral range of the whispering-gallery TE01 mode in the MAI silicon disk is 13.9 nm. With a fitting by a damped oscillator model, an intrinsic Q factor of 8.1×10^4 and a coupling Q factor of 7.5×10^4 are obtained [see Fig. 3(b)]. The corresponding FWHM of the ditch is about 43 pm. The narrow linewidth of the disk resonator guarantees on–off switching of the transmitted light by a small temperature variation.

At first, the temperature dependency of the resonance wavelength of the disk was measured by increasing the temperature of the whole sample from 20°C to 35°C with

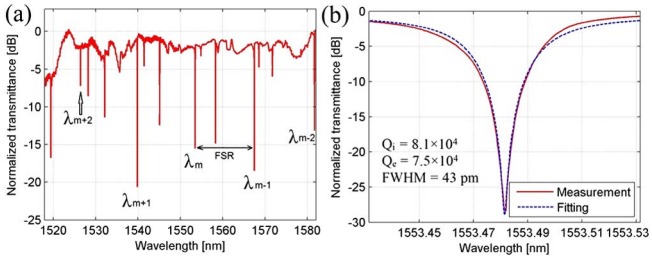

Fig. 3. (a) Measured transmission spectrum of the MAI Si disk. (b) Measured transmission spectrum of the MAI Si disk around 1553.48 nm, fitted by a damped oscillation model.

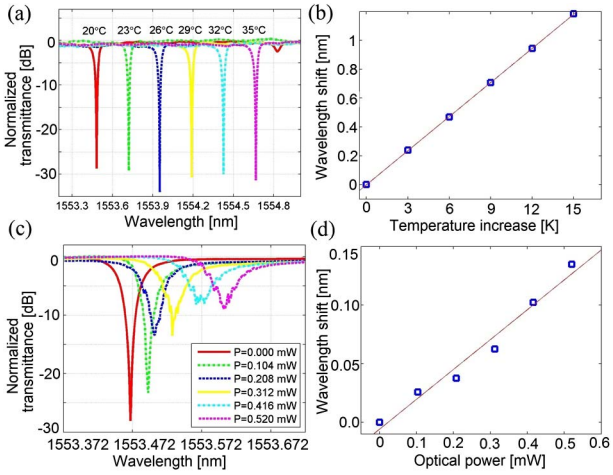

Fig. 4. (a) Measured transmission spectra of the MAI Si disk operating at a temperature ranging from 20°C to 35°C. (b) Wavelength shift versus temperature increase of the whispering-gallery mode in the MAI Si disk. (c) Measured transmission spectra of the MAI Si disk optically pumped by a continuous-wave laser beam with power on sample ranging from 0.00 to 0.52 mW. (d) Wavelength shift versus pumping optical power of the photothermally tuned MAI Si disk.

a TEC. The thermally tuned transmission spectra of the disk are shown in Fig. 4(a), where the resonance wavelength redshifts with increasing the device temperature. The measured thermal wavelength shift ratio $(d\lambda_m/dT)$ by linear fitting is around 78.8 pm/K, as shown in Fig. 4(b). Then we photothermally tuned the microdisk by linearly increasing the power of the pump laser, as shown in Fig. 4(c). The measured total pump power on the sample (P_0) is from 0.00 to 0.52 mW. Figure 4(d) shows the relation of wavelength shift $(\Delta\lambda_m)$ versus pump power (P_0); the fitted slope $(d\lambda_m/dP_0)$ is about 0.255 nm/mW. This also indicates that the pump power derivative of temperature increase is about 3.24 K/mW for the photothermally tuned MAI microdisk. Broadening of the measured transmission resonant ditch in Fig. 4(c) should be caused by the wavelength fluctuation combined with time average in the measurement and partly by the loss caused by the free-carrier excited by pump light, but it does not affect the switching performance.

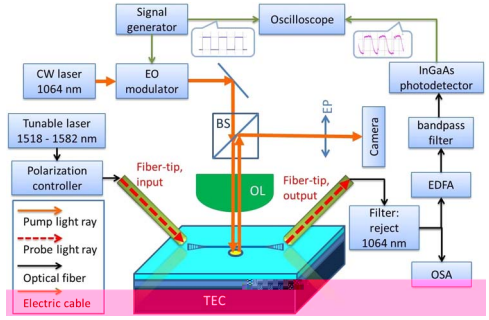

Fig. 5. Schematic of the experimental setup for measuring the photothermal tuning of MAI disk. CW laser, continuous wave laser; EO, electro-optic; BS, beam splitter; OL, objective lens; EP, eyepiece; EDFA, erbium-doped fiber amplifier; OSA, optical spectrum analyzer; TEC, thermoelectric controller.

The temporal response of the fabricated device was then measured with a square-wave modulated pump light. Figure 5 shows the schematic of the experiment setup. As shown in the figure, by the input fiber tip (left), the linearly polarized probe light from a tunable laser is coupled to the Si waveguide assisted by a shallow-etched grating. After interaction with the MAI disk resonator, the probe light is diffracted by the grating on the other side and collected by the output fiber tip (right). In this dynamic response measurement, the wavelength of the probe light is fixed at a value slightly larger than resonance peak, but within the FWHM of the transmission ditch. The transmitted light is amplified by an erbium-doped fiber amplifier followed by a narrow linewidth filter. The amplified light is converted to an electric signal by an InGaAs photodetector. The MAI disk is tuned by a focused pump laser beam from the objective lens. The temporal response of the transmitted optical signal is monitored by an oscilloscope. The 1064 nm wavelength pump light is modulated by an electro-optic modulator, following a square-wave variation in time. The varying pump light induces a periodic change in the disk-resonator's resonance wavelength. The measured temporal response of the MAI disk is shown in Fig. 6, with a modulation period ranging from 40 to 4 μs and a 50% duty cycle. A relatively fast temporal response with a rise time τ_r of 2.0 μs and a fall time τ_f of 2.6 μs is achieved. For dynamic on–off switching, the power of the pump beam on the sample surface is about 0.5 mW, so the product of switching power and response time is only about 1.3 mW · μs. Compared with the rise time, the longer fall time is due to the fact that it takes time for heat to be dissipated from the Si disk to the substrate, as limited by the low thermal conductivity of SiO_2 [1.4 W/(m · K)]. In our demonstrated device, the top Si layer is totally etched to form the Si microdisk. One can actually partially etch away the Si layer for forming a rib-type Si microdisk. Owing to the fact that the thermal conductivity of Si [142 W/(m · K) for bulk Si] is much larger than that of SiO_2, it is possible to improve the fall time as the residual

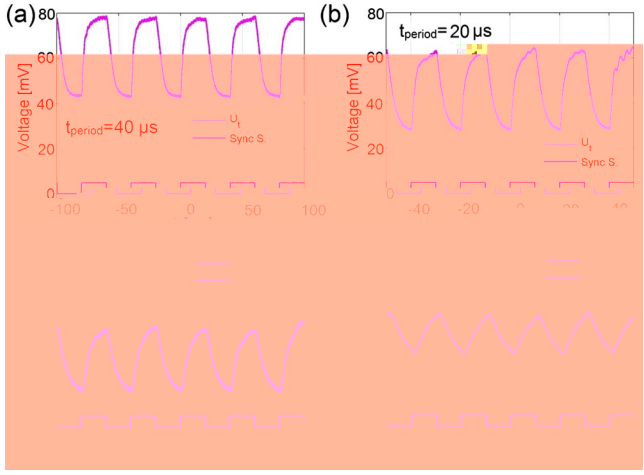

Fig. 6. Measured temporal transmitted optical signal of the MAI Si disk resonator, pumped by a square-wave modulated beam with duty cycle of 50% and periods of (a) 40 μs, (b) 20 μs, (c) 10 μs, and (d) 4 μs.

top Si film can quickly dissipate heat away from the disk [25].

In our proof-of-concept demonstration, we have used the most elementary geometry of a microdisk resonator integrated with a MIM absorber. Optimizations can be made to improve the performance. For instance, compared with the electrically driven heater, the size of a MIM absorber can be further reduced (even to submicrometer scale). As a consequence, the size of the silicon disk can be reduced, together with the total heat capacity of the device, accordingly. For example, the diameter of the Si microdisk and the integrated MIM absorber can be reduced to 3.0 and 1.0 μm, respectively. If a hybrid plasmonic waveguide is applied, the diameter can be further reduced to be lower than 1.0 μm [26,27]. In such a way, photothermal all-optical switches with even more compact size and improved performance can be achieved. In addition, with only minor adjustments in the fabrication process, the absorption property of the MIM absorber can be tailored to incorporate the specifications of different pump sources, e.g., lasing wavelength, linewidth, polarization, and beam profile [22,24].

In summary, a novel all-optical switch based on a plasmonic light absorber is proposed and experimentally demonstrated. The MIM light absorber was integrated directly on top of the Si microdisk resonator to minimize the overall heat capacity of the device and maximize the heat conduction from the heat source to the substrate. Therefore, the temporal response of the proposed structure is relatively fast with a rise/fall time of around 2.0 μs, which is comparable with state-of-the-art values in TO switches based on electrical heaters. Comparatively, plasmonic light absorbers have advantages such as compact size, low heat capacity, highly efficient light-to-heat conversion, and an elementary fabrication process. Photothermal optical switching via this approach can be important for applications, where contactless light switching or routing is needed.

The authors would like to thank Dr. Walter Margulis (Acreo AB, Sweden), Yu Xiang (Department of Integrated Devices and Circuits, KTH) and Prof. Urban Westergren (Department of Materials and Nano Physics, KTH) for their help with the characterization setup. This work was supported by the Swedish Research Council (VR), VR's Linnaeus Center in Advanced Optics and Photonics (ADOPT). M. Q. acknowledges support by the National Science Foundation of China (grants nos. 61275030, 61205030, and 61235007).

†Both authors contributed equally to this work.

References

1. B. Jalali and S. Fathpour, J. Lightwave Technol. **24**, 4600 (2006).
2. R. Soref, IEEE J. Sel. Top. Quantum Electron. **12**, 1678 (2006).
3. A. Liu, R. Jones, L. Liao, D. Samara-Rubio, D. Rubin, O. Cohen, R. Nicolaescu, and M. Paniccia, Nature **427**, 615 (2004).
4. L. Liao, A. Liu, J. Basak, H. Nguyen, M. Paniccia, D. Rubin, Y. Chetrit, R. Cohen, and N. Izhaky, Electron. Lett. **43**, 1196 (2007).
5. G. T. Reed, G. Mashanovich, F. Y. Gardes, and D. J. Thomson, Nat. Photonics **4**, 518 (2010).
6. H. Park, A. Fang, S. Kodama, and J. Bowers, Opt. Express **13**, 9460 (2005).
7. A. Fang, H. Park, R. Jones, O. Cohen, M. Paniccia, and J. Bowers, IEEE Photon. Technol. Lett. **18**, 1143 (2006).
8. D. Liang and J. E. Bowers, Nat. Photonics **4**, 511 (2010).
9. G. Masini, L. Colace, and G. Assanto, Appl. Phys. Lett. **82**, 2524 (2003).
10. G. Dehlinger, S. Koester, J. Schaub, J. Chu, Q. Ouyang, and A. Grill, IEEE Photon. Technol. Lett. **16**, 2547 (2004).
11. L. Chen and M. Lipson, Opt. Express **17**, 7901 (2009).
12. Q. Xu, B. Schmidt, S. Pradhan, and M. Lipson, Nature **435**, 325 (2005).
13. V. Almeida, C. Barrios, R. Panepucci, and M. Lipson, Nature **431**, 1081 (2004).
14. M. Harjanne, M. Kapulainen, T. Aalto, and P. Heimala, IEEE Photon. Technol. Lett. **16**, 2039 (2004).
15. M. Geis, S. Spector, R. Williamson, and T. Lyszczarz, IEEE Photon. Technol. Lett. **16**, 2514 (2004).
16. A. Densmore, S. Janz, R. Ma, J. H. Schmid, D.-X. Xu, A. Delage, J. Lapointe, M. Vachon, and P. Cheben, Opt. Express **17**, 10457 (2009).
17. M. R. Watts, W. A. Zortman, D. C. Trotter, G. N. Nielson, D. L. Luck, and R. W. Young, in *Conference on Lasers and Electro-Optics/International Quantum Electronics Conference* (Optical Society of America, 2009), paper CPDB10.
18. P. Dong, W. Qian, H. Liang, R. Shafiiha, D. Feng, G. Li, J. E. Cunningham, A. V. Krishnamoorthy, and M. Asghari, Opt. Express **18**, 20298 (2010).
19. J. Gosciniak and S. I. Bozhevolnyi, Sci. Rep. **3**, 1803 (2013).
20. M. R. Watts, J. Sun, C. DeRose, D. C. Trotter, R. W. Young, and G. N. Nielson, Opt. Lett. **38**, 733 (2013).
21. J. Sun, E. Timurdogan, A. Yaacobi, E. S. Hosseini, and M. R. Watts, Nature **493**, 195 (2013).
22. J. Hao, J. Wang, X. Liu, W. J. Padilla, L. Zhou, and M. Qiu, Appl. Phys. Lett. **96**, 251104 (2010).
23. X. Liu, T. Starr, A. F. Starr, and W. J. Padilla, Phys. Rev. Lett. **104**, 207403 (2010).
24. M. Yan, J. Opt. **15**, 025006 (2013).
25. A. Rickman, G. Reed, and F. Namavar, J. Lightwave Technol. **12**, 1771 (1994).
26. F. Lou, Z. Wang, D. Dai, L. Wosinski, and L. Thylen, in *International Photonics and Optoelectronics Meetings/Information Optoelectronics, Nanofabrication and Testing* (Optical Society of America, 2012), paper IF2A.
27. F. Lou, M. Yan, L. Thylen, M. Qiu, and L. Wosinski, Opt. Express **22**, 8490 (2014).